eVTOL Rotor Noise in Ground Effect

Brendan Smith PhD Student
Richard Healy PhD Student
Dr. Farhan Gandhi Redfern Chair, Director
Anastasios Lyrintzis Distinguished Professor & Chair

Center for Mobility with Vertical Lift (MOVE)
Rensselaer Polytechnic Institute
Troy, New York, United States

Department of Aerospace Engineering
Embry-Riddle Aeronautical University
Daytona Beach, Florida, United States

ABSTRACT

This study examines a hovering three-bladed two-rotor system in close operation to the ground. The rotor pair is oppositely phased and is examined for two heights, H/D = 1 and H/D = 0.5. Loads for these rotors are generated using the CFD solver AcuSolve, as well as the Rensselaer Multicopter Analysis Code (RMAC). The loads generated using CFD include aerodynamic interactions from inter-rotor effects and ground-rotor effects. These loads are coupled to the acoustic propagation PSU-WOPWOP code for acoustic predictions at an observer grid located at "ear height" from the ground. Rotors are also added below the ground to simulate perfect acoustic ground reflections. The simulation results show that the noise signals from the rotorshave a distinct directivity pattern of six locations of high noise and six locations of low noise caused by the rotor phasing. The introduction of aerodynamic interactions increases loading noise and has a significant effect on the high frequency noise content. These effects are amplified for the H/D = 0.5 case as the interactions are stronger. Ground reflections increase noise across the observer grid, and further enhance the high frequency noise generated by the interactional aerodynamic loads.

1. INTRODUCTION

Due to the increasing viability of distributed electric propulsion at a larger scale, there has been a large interest in the development of multi-rotor electric VTOL (eVTOL) aircraft. Small-scale battery powered multi-copters have been available for videography and recreational use for quite a while. In addition, there has been a recent interest for larger eVTOL to support the Urban Air Mobility (UAM) as, for example, described by the Uber Elevate Program (Ref. 1) and the NASA UAM Grand Challenge (Ref. 2). A key challenge to the success of UAM is the community acceptance of the noise generated by these eVTOL aircraft, which will be operating in suburban and urban areas of high population density.

Through many decades of comprehensive research, the noise characteristics of conventional helicopters is well understood. To take an example, Ref. 3 details key noise sources for conventional helicopters – thickness noise, loading noise, high-speed impulsive noise, blade-vortex interaction noise, and broadband noise – and the conditions for which they are dominant. However, there remains a lack of similar comprehensive understanding for eVTOL aircraft. Although the types of the noise sources remain the same, their relative importance changes and low noise conditions need to be studied

Several research groups have addressed this gap in the level of understanding. Researchers at NASA Langley Research Center (LaRC) have conducted many experiments coupled with associated simulations for small, fixed-pitch, variable RPM rotors and their assemblies (Refs. 4-8). Through these studies they have examined key noise sources, rotor-airframe interaction effects, broadband noise, and how phase synchronization affects rotor noise. In addition, there have been other studies examining the acoustics on small, fixed-pitch, variable-RPM single rotor, quadcopters, and hexacopters reported in Refs. 9-11.

Along with experimental work, there have been several simulation studies on multi-rotor aircraft in recent years. Unlike the experiments on small rotors discussed above, these simulations focused more heavily on larger multi-rotors aircraft that are more typical of UAM missions. Passe and Baeder (Ref. 12) studied the effect of certain rotor design parameters and boom shadow on eVTOL aeroacoutsic characteristics for hover conditions. Another important area of study is the aeroacoustic impact of propeller-wing, -body, -duct, and -boom interactions (Refs. 13-15). Also, broadband noise of eVTOL rotors (Refs. 18,19) has been highlighted as an important noise source (Ref. 11).

A key difference between the proposed multi-copter designs and conventional helicopters is the close proximity of rotors that induces a significant aerodynamic interaction. To address this, studies have looked at interactional effects on aerodynamics and aeroacoustics utilizing both Vortex Particle Methods (VPM) and CFD for side-by-side as well as stacked rotor configurations (Refs. 19-22).

Presented at the Vertical Flight Society's 77th Annual Forum & Technology Display, Virtual, May 10-14, 2021

While many studies have expanded the understanding of different noise aspects of eVTOL configurations, there has been a limited consideration of the effect of the ground. The current study will examine eVTOL noise for near ground operations of a multi-rotor system.

2. ANALYSIS

2.1 GEOMETRIC SETUP

Airloads for the rotors are generated using CFD, utilizing the geometry given in Table 1. The two rotors are arranged in a side-by-side configuration hovering near the ground, phased opposite one another at 60° phasing. The hub-to-hub separation is 2.5R, and there are two cases of ground distance for the airloads: H/D = 1, H/D = 0.5. The geometric configuration of the side-by-side system is given in Figure 1. Along with the CFD loads, airloads are also generated using the Rensselaer Multicopter Analysis Code, RMAC (Ref. 23). RMAC is a physics-based comprehensive flight-simulation analysis tool which uses blade-element-theory in conjunction with a 10-state Peters-He finite-state dynamic wake model to calculate the sectional blade loads. These loads are used to provide a comparison which does not account for interaction between the rotor pair and between the rotors and the ground.

Table 1: Geometric parameters of simulation rotor

Parameter	Value
Radius	0.8382 m (2.75 ft)
Disk Loading	5 lb/ft^2
RPM	1600
Number of Blades	3
Root Pitch	20°
Twist Rate	-10° per span
Chord	0.0834 m (0.274 ft) [No Taper]
Root Cutout	0.2 R
Airfoil	NACA 23012

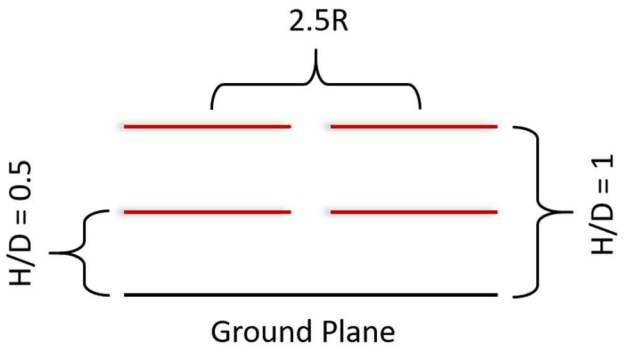

Figure 1: Geometric setup of the two rotor system

2.2 CFD ANALYSIS

The CFD simulations are conducted using the commercial Navier-Stokes solver AcuSolve which uses a stabilized 2nd order upwind finite element method. AcuSolve simulations for a Straight Up Imaging (SUI) Endurance rotor were previously shown to compare well against experimental results (Ref. 24). For a 2-rotor unit, the computational domain is shown in Figure 2. The nonrotating volume is a rectangular prism with sides and top boundaries set to outflow with backflow conditions enabled. This allows for flow in either direction across the boundary with zero pressure offset. The bottom surface is set to no-slip condition in a weak fashion with a log-law based wall function (Ref. 25) which acts like a wall model (Ref. 26) without the impractical computational cost associated with resolving the ground boundary layer. Around each rotor there is a cylindrical rotating volume with interface surfaces that pass information to and from the non-rotating volume.

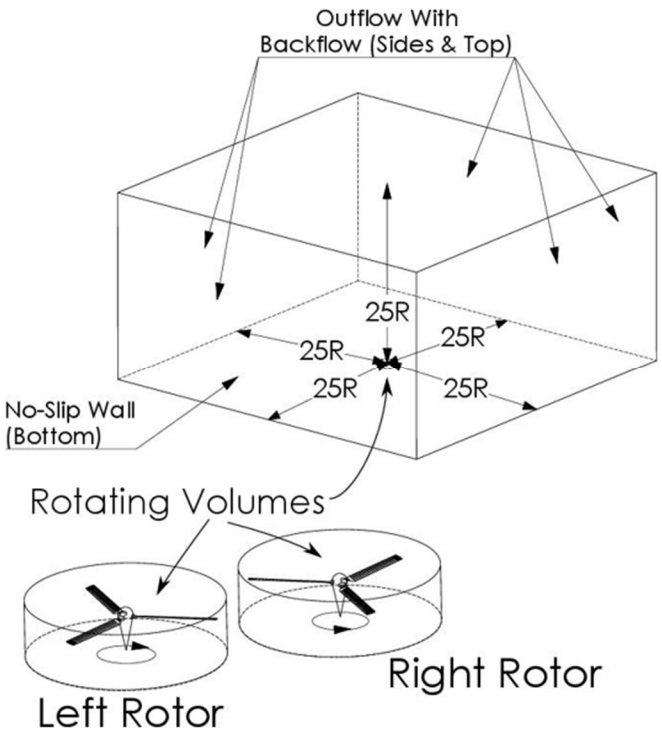

Figure 2: Diagram of CFD computational domain

The computational domain is discretized using an entirely unstructured, tetrahedral elements. On each blade, the surface mesh is set to ensure 200 elements around the airfoil contour, with refinement along the leading and trailing edges. The boundary layer in the wall-normal direction is highly resolved, with the first element height set to ensure a $y+ < 1$. A portion of the blade surface mesh and a clipped slice of the boundary layer mesh is shown in Figure 3. Surrounding the rotors, and extending to the ground below, a set of cylindrical

wake refinement zones are prescribed as detailed in Figure 4. A boundary layer mesh is near the ground to capture the necessary viscous effects. The entire computational domain is comprised of approximately 170 million elements for side-by-side cases, with 50 million in each rotating volume, and 70 million in the surrounding non-rotating volume. These rotor mesh parameters have been used in previously published AcuSolve rotorcraft simulations and have been found to provide good spatial resolution (Refs. 27 and 28).

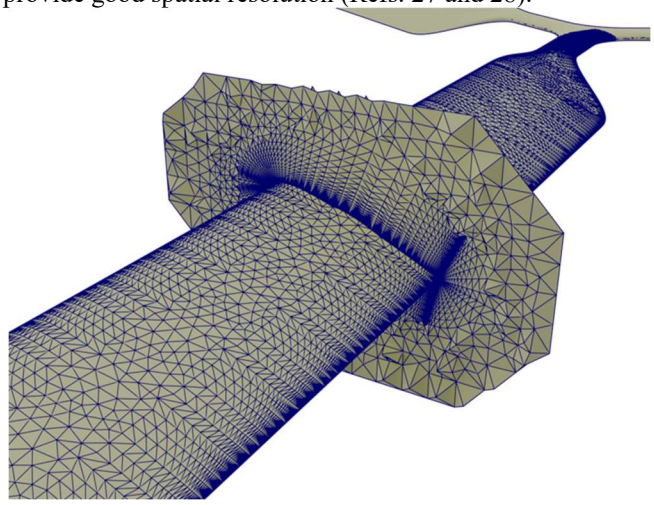

Figure 3: Blade surface mesh viewed near mid span, and a chordwise slice showing the boundary layer mesh in the wall-normal direction

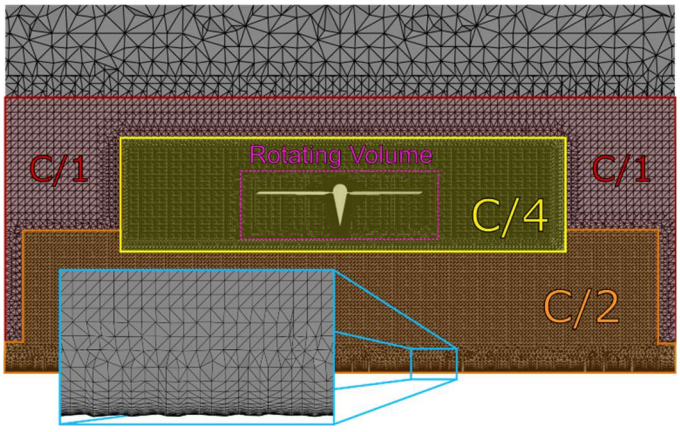

Figure 4: Cross-section of wake mesh refinement, with element size for each zone denoted by the fraction of blade chord length

A detached eddy simulation (DES) is used with the Spalart-Allmaras (SA) turbulence model for all simulations. Forty revolutions with timesteps corresponding to 10° of blade motion are first simulated to develop the wake quickly, followed by at minimum 5 revolutions with 1° timesteps. All runs are performed on 8 24 core AMD Epyc 7451 processors, part of the Center for Computational Innovations (CCI) at Rensselaer Polytechnic Institute. Additional CFD methodology details can be found in Ref. 29.

2.3 ACOUSTIC ANALYSIS

The blade loads for all the rotor cases are provided as input to PSU-WOPWOP (Ref. 30), an acoustic propagation code based on the numerical implementation of Farassat's Formulation 1A of the Ffowcs Williams and Hawkings equation. Both the CFD and RMAC provide chordwise compact loads to PSU-WOPWOP, and only tonal noise from thickness and loading sources are considered in the acoustic analysis. The user selects observer locations where the acoustic time pressure history will be calculated by PSU-WOPWOP based on the specified rotors, whose location and phasing are also selected by the user. For this study, the observers are placed at a vertical distance of 5.5 ft (1 rotor diameter) above the ground, which is shown in Figure 5 for a single rotor. This height was chosen as it is close to "ear height" for any humans in the proximity of the aircraft. This means that for the case of H/D = 1, the observer will be in plane with the rotor, and for H/D = 0.5, the rotor will be vertically lower than the observer height. Noise is also considered for rotors operating out of ground effect (OGE), in which case the observer is positioned in plane with the rotor as demonstrated in the left most portion of Figure 5. For the two-rotor system, the observers are arranged as shown in the top view in Figure 6, again at the same height described previously. The observers marked A, B, C, etc. are locations of peak and low noise that are discussed in the results section.

Along with the aerodynamic influence of the ground plane, the effect of acoustic reflections off the ground needs to also be considered. To achieve this, a mirrored rotor (flipped z-axis and opposite spin direction) is placed below the ground at the same distance as the above-ground rotor. This is demonstrated in Figure 7, which shows the source rotor Z, the reflection rotor Z', and their relative distance to an observer for H/D = 0.5. In the case of the two-rotor system, each above-ground rotor has their own reflection rotor and using superposition the acoustic time pressure history can be calculated for any given observer, allowing the SPL (frequency spectrum) and OASPL in dB and dBA to be calculated. Acoustic reflections are run for cases with and without aerodynamic interaction, to provide a better comparison for the effects of interaction with reflections.

To demonstrate that RMAC provides a good approximation for OGE CFD loads, the acoustic pressure time history and OASPL are compared at observers for both the H/D = 1 and H/D = 0.5 setups shown in Figure 7 (center and right) for a single rotor. The overall acoustic pressure is shown in Figure 8, with the results of RMAC and the OGE

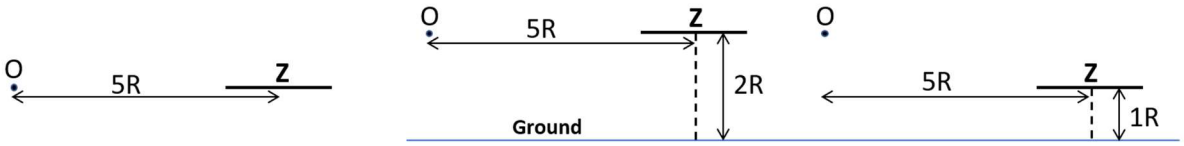

Figure 5: Side-view of rotor, ground, and observer location for (left) out of ground effect (middle) H/D = 1 (right) H/D = 0.5

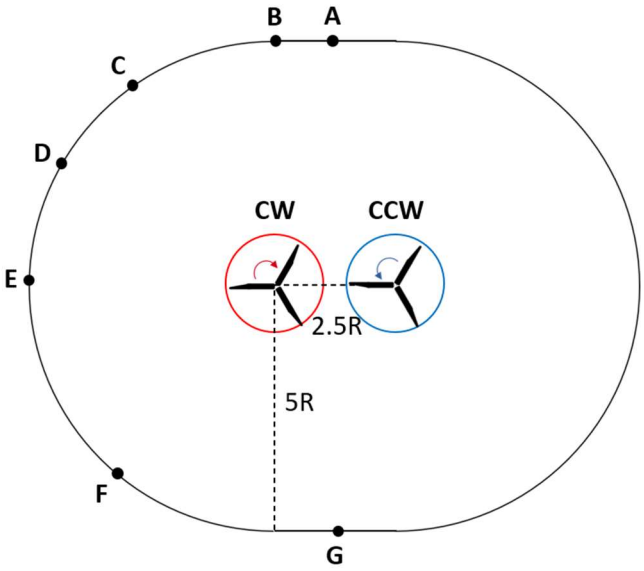

Figure 6: Top view of two-rotor system with observer grid

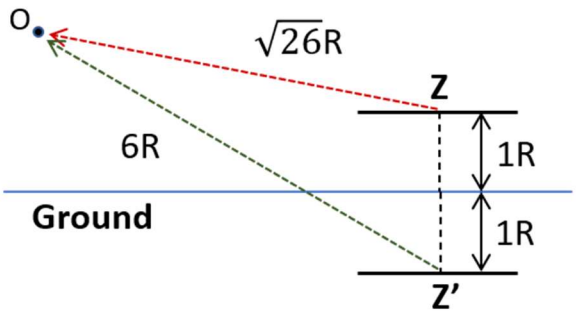

Figure 7: Setup of ground reflections for H/D = 0.5

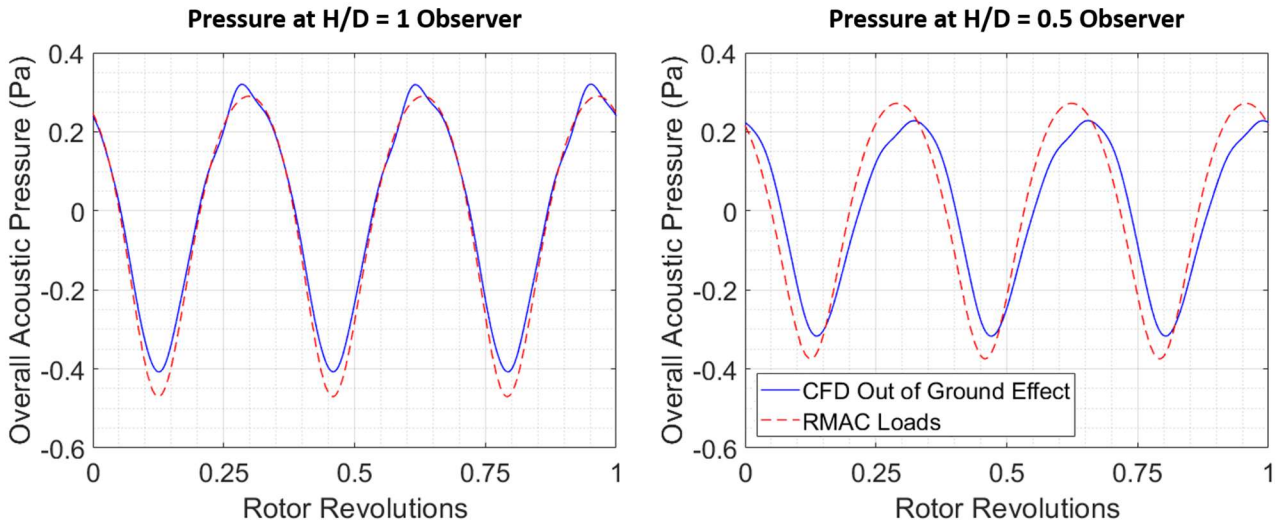

Figure 8: Time pressure history for single rotor CFD out of ground effect (OGE) and RMAC loads at H/D = 1 and H/D = 0.5 observers

CFD showing very good correlation. There are slight differences in magnitude, but when considering the OASPL noise in dB, the maximum difference is 0.7 dB for H/D = 0.5 and 0.2 dB for H/D = 1 observers, which shows RMAC is a good substitution for OGE CFD loads. (Please note that H/D values just refer to the observer location in figure 5, as all calculations are OGE).

3. RESULTS

3.1 Two Rotors at H/D = 1

Figure 9 exhibits the OASPL noise for the observer grid shown in Figure 6 for the case of H/D = 1, with the dashed lines indicating the locations of points A, B, C, D, E, F, and G. Since RMAC does not account for aerodynamic (wake) interaction, these results are just representative of acoustic interactions between rotors and between the rotor and ground. The noise (OASPL) of the RMAC and CFD loads shows the same directivity pattern, with 6 directions of peak noise and 6 directions of low noise due to the 60° phasing between rotors. The noise calculation does not include ground reflections. The main reason for the directivity pattern is the phasing of the signals from the two rotors. For example, for point A (and all points at an equal distance from the two rotors including point G), the signals are 60° apart due to the phase difference of the two 3-bladed rotors. Thus, the signals from the two rotors arrive out of phase (60° apart) creating a low in OASPL and 6 peaks per rotor revolution. However, at point B the signals from the two rotors arrive with the same phase and add up to create a maximum. The difference between these peaks and lows is at most 13.5 dB for the RMAC loads and 14 dB for the CFD loads, showing good agreement in the overall magnitude. While the RMAC results are symmetric between the left and right side of the vehicle, the CFD loads show a slight difference, with the most pronounced changes seen in the two low points on either side. There is a difference of 1 dB between points E and C and their mirrored locations. These noise changes are driven by the difference between individual rotor loads caused by the aerodynamic interactions, due to the slight asymmetry of the aerodynamics interactions in the CFD results. However, the OASPL values are very close.

To further examine differences between the cases the acoustic time pressure history is inspected for one rotor revolution. Figures 10 and 11 show a breakdown of the acoustic time pressure history at Points A and B for the RMAC and CFD cases. Beginning first with the RMAC case at Point A, the resulting pressure signal is 6/rev dominant due to the fact that this point sits equidistant from oppositely phased rotors, so the resulting signal shows a dominant frequency equal to the total number of rotor blades of the two-rotor configuration. When compared to the signal generated by CFD loads, a 6/rev dominant signal is still observed, but there is a high frequency content that is observable in the loading noise signal, due to interference effects. Thickness noise remains the same because the geometry definition is shared between cases. Thickness noise is the dominant noise signal, and since the interference effect on the loading noise is not strong, the two points have a similar OASPL value. Point B shows a 3/rev signal, indicating a point of constructive interference between rotor signals. Again, the CFD loading noise signal shows some higher frequency content, but the effect of aerodynamic interference is not large enough to cause significant changes in the signal.

Next, we examine the effect of introducing reflections from the ground on the noise signal for the same observer grid, achieved by placing mirror image rotors at an equal distance below the ground as detailed in the analysis section. The OASPL noise for the observer grid for both the RMAC and CFD cases is shown in Figure 12. On these graphs we show the OASPL with and without ground reflections to demonstrate their influence on the noise signature. Beginning with the RMAC loads, we can see that the introduction of reflections increases the noise across the observer grid, while preserving the directivity pattern that was shown previously. This noise increase is most pronounced at high noise locations, with the maximum increase being 2 dB at point F and at point F's mirrored location. The CFD case also sees an increase in noise, but a larger maximum increase of 5 dB is observed at point G. The difference between the noise observed on the left and right side of the configuration is more pronounced when including ground reflections because the added aerodynamic interference breaks the symmetry of the two rotor wakes further. While previously (i.e. without reflections) the maximum difference between sides was found to be 1 dB, this increases to 4 dB for the lows observed at point C and its mirrored location. For the case with reflections, the effects of the interactional aerodynamics have a larger influence on the OASPL when ground reflections are included, but overall, the noise is still comparable between cases.

To examine how the reflections affect the pressure time history, Figures 13 and 14 show the noise source breakdown of the acoustic pressure over a single rotor revolution at points A and B for both the RMAC and the CFD cases, with the ground reflections included. The pressure signal at point A for the loads without aerodynamic interactions (RMAC) looks very similar in nature to the case without reflections, with a smooth 6/rev signal where thickness noise is the dominating noise source. In contract, when using the CFD loads, the signal does not collate well with the cases without reflection (Figures 10 and 11). The signal is still 6/rev dominant, but the higher frequency noise content is much more pronounced, when compared to the signal without ground reflections. The loading noise is much stronger than the thickness noise over some of the signal range, with loading noise peaks and troughs that are twice the magnitude of the thickness signal.

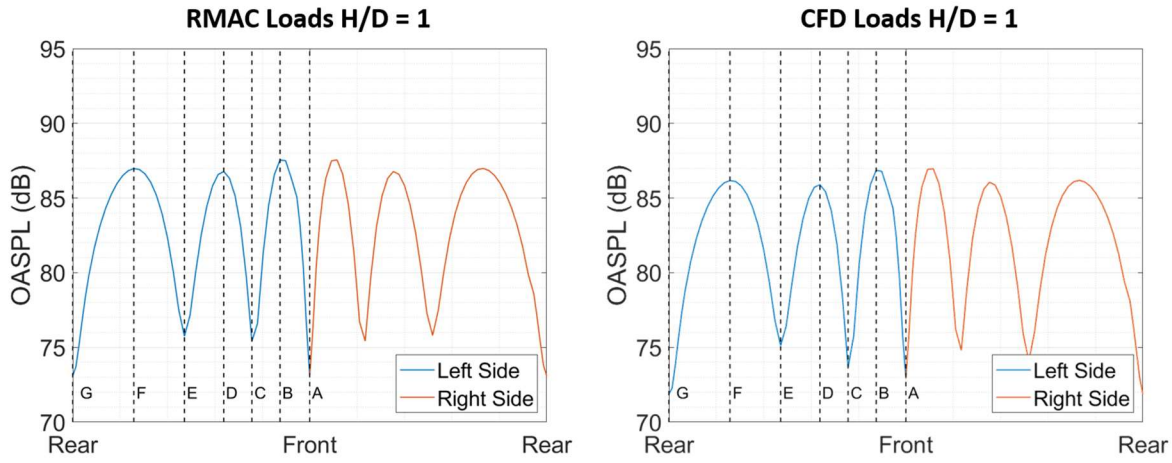

Figure 9: OASPL dB noise at observer grid for H/D = 1, no ground reflections

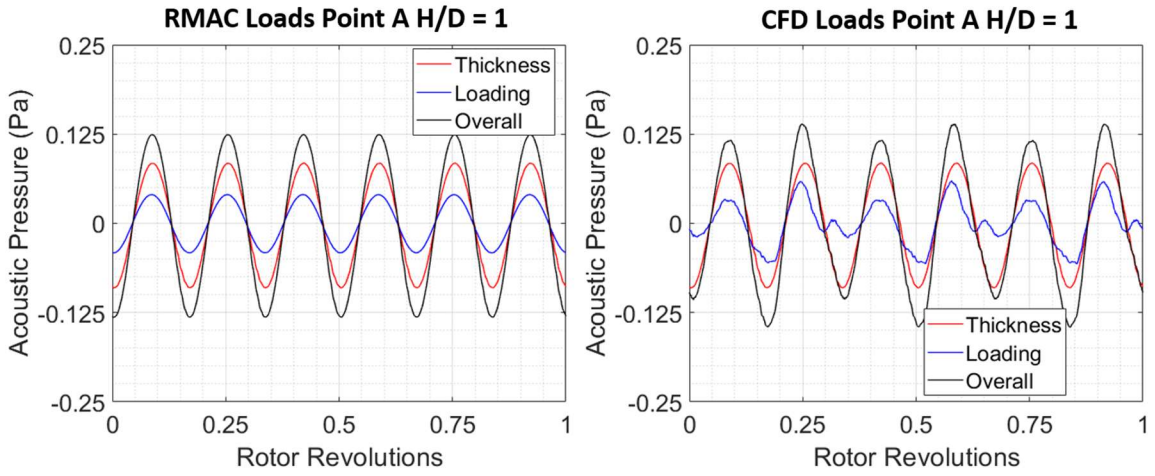

Figure 10: Acoustic pressure time history for H/D = 1 at point A (left) RMAC loads (right) CFD loads, no ground reflections

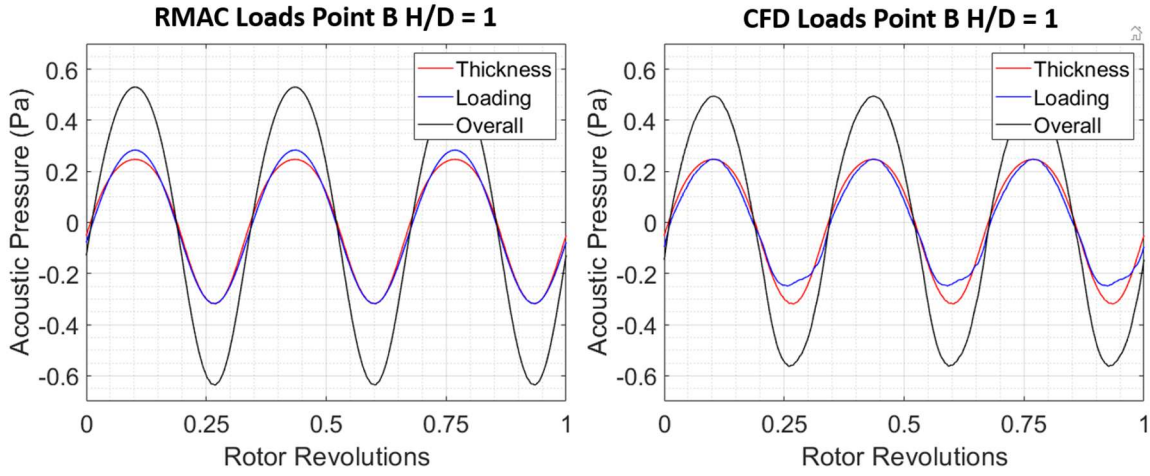

Figure 11: Acoustic pressure time history for H/D = 1 at point B (left) RMAC loads (right) CFD loads, no ground reflections

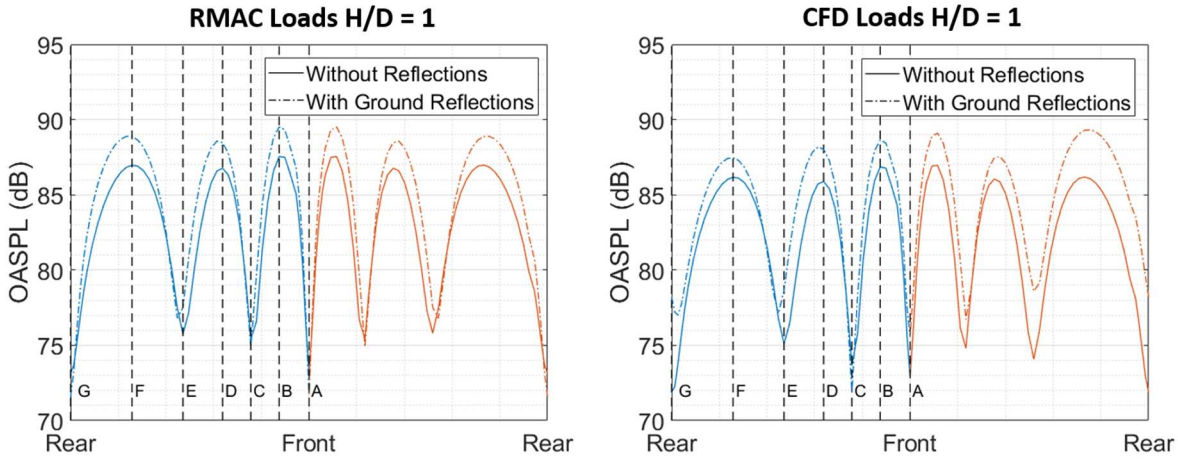

Figure 12: OASPL dB noise at observer grid for H/D = 1, including ground reflections

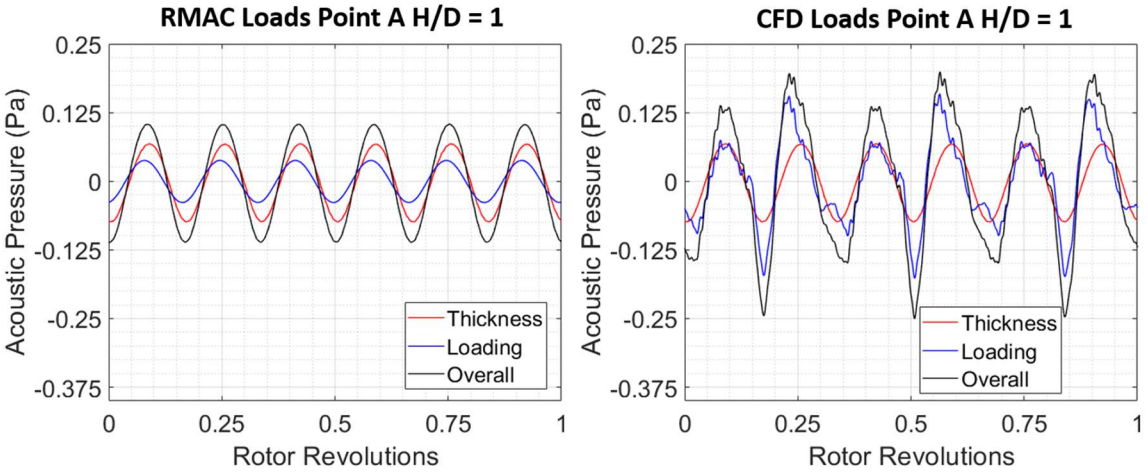

Figure 13: Acoustic pressure time history for H/D = 1 at point A (left) RMAC loads (right) CFD loads, including ground reflections

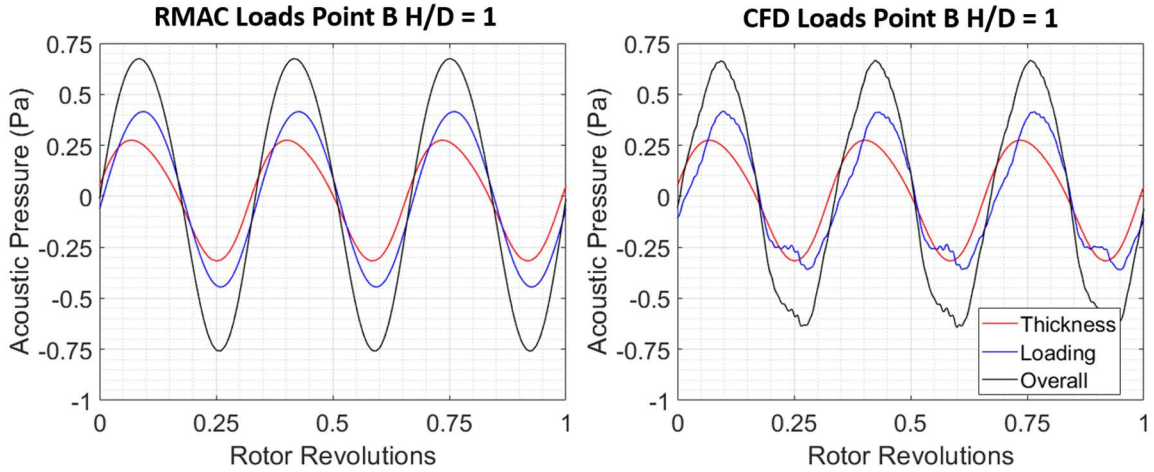

Figure 14: Acoustic pressure time history for H/D = 1 at point B (left) RMAC loads (right) CFD loads, including ground reflections

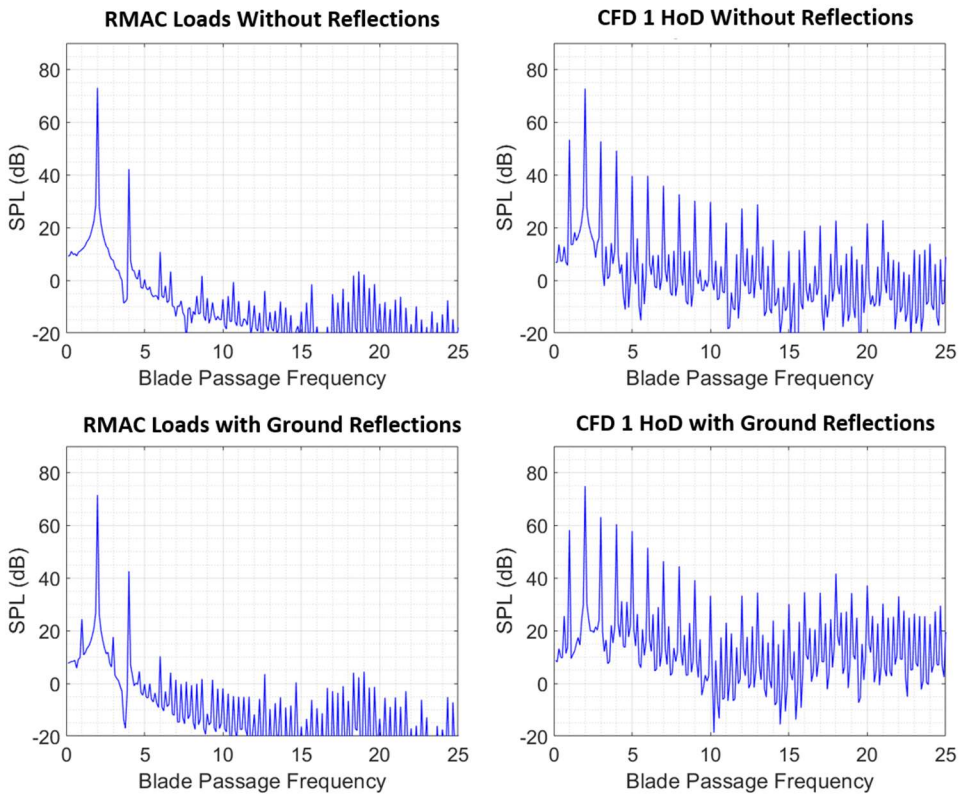

Figure 15: SPL breakdown for Point A H/D = 1 (top left) RMAC loads no reflections (top right) CFD loads no reflections (bottom left) RMAC loads with ground reflections (bottom right) CFD loads with ground reflections

The comparison at point B falls more in line with what was observed without ground reflections. The signal is 3/rev with loading noise now more dominant than thickness noise. Unlike point A, the higher frequency noise caused by aerodynamic interactions does not change the overall shape of the signal.

While the OASPL in dB is comparable, as indicated by Figure 12, the frequency content could be different. Figure 15 shows the Sound Pressure Level (SPL) of the noise signal as a function of blade passage frequency (BPF = 80 Hz) for both cases at point A, with and without reflections. The RMAC loads show a large dominant peak located at the 2nd BPF. This corresponds with what is observed in the pressure signals seen in Figures 10 and 13, which show a 6/rev signal. The CFD case both with and without reflection still shows the dominant noise peak coming at the 2nd BPF, resulting in a similar OASPL. There is an additional peak at 1 BPF due to the wake interference. However, the main difference is that the high frequency content due to the aerodynamic interaction is pronounced in the CFD case, with peaks showing through the 25th BPF. The high frequency noise content may have an effect in the way it is perceived by humans, as hearing is biased towards high frequencies (>1000 Hz). Table 2 gives the values for OASPL dB, OASPL dBA, and high frequency noise (6th to 25th BPF) in dB for points A and B. Data are shown for the RMAC and CFD loads with and without ground reflections. For the two cases without ground reflections, both OASPL dB and dBA values are comparable, with no more than 1 dB or dBA difference observed. This can be attributed to the fact that the 2nd BPF spike is dominant for both cases despite of the A-weighting biasing towards human hearing at higher frequencies. However, when considering just the higher frequency content, the 6th to 25th BPF, this is no longer the case. For this frequency range, just the aerodynamic

Table 2: dB, dBA, and 6th to 25th BPF Noise for Points A and B, H/D = 1

RMAC Loads no Reflections

Point	dB	dBA	6th to 25th BPF
A	73.1	59.9	13.1
B	86.3	64.2	23.7

CFD Loads no Reflections

Point	dB	dBA	6th to 25th BPF
A	72.9	59.8	40.1
B	85.5	63.5	44.0

RMAC Loads with Ground Reflections

Point	dB	dBA	6th to 25th BPF
A	71.7	58.3	15.4
B	89.4	65.9	25.9

CFD Loads with Ground Reflections

Point	dB	dBA	6th to 25th BPF
A	75.5	63.7	51.1
B	88.5	65.6	49.9

interactions in the CFD cause a increase of 27 dB at point A and 20.7 dB at point B. Adding ground reflections increases the difference in dBA noise, with the A-weighted noise at point A being 5.4 dBA higher as opposed to 0.1 dBA lower when there are no ground reflections. Also, the increase in the high frequency noise is greater, with a difference of 35.7 dB at point A and 24 dB at point B, showing that including ground reflections enhances the high frequency effects of the aerodynamic interactions. The interaction between the two rotor wakes and the two wakes and the ground breaks down parts of the wake and creates additional high frequencies This wake structure and breakdown for H/D = 1 is shown through a snapshot of the vorticity magnitude in Figure 16. However, the effect on the high frequency content due to the presence of aerodynamic interactions is higher than the effect due to the presence of reflections. In Summary, while aerodynamic interactions may not affect the noise when just considering OASPL dB, there is a significant effect on high frequency noise, which may influence how human observers perceive it.

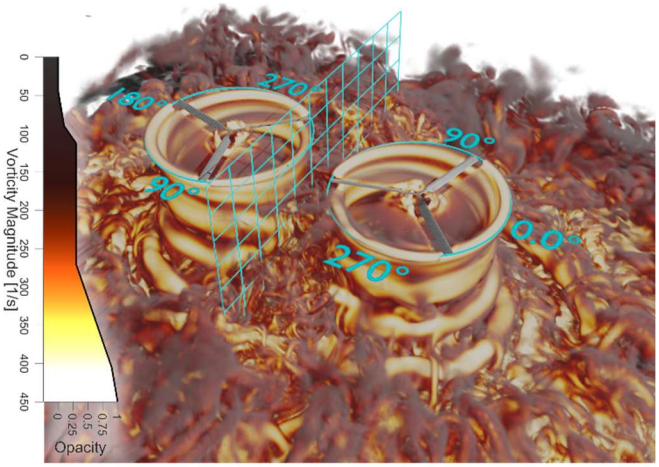

Figure 16: Rotor wake vorticity diagram for H/D = 1

3.2 Two Rotors at H/D = 0.5

This section compares loads with and without aerodynamic interaction for rotors closer to the ground, at H/D = 0.5. As detailed in Ref. 29, the interactional effects on loading are much more pronounced for H/D = 0.5 than for H/D = 1. The observer grid now sits 1R above the rotors at the same "ear height" location, as shown in Figure 6. The effect of the elevation angle compared with the rotation plane for the H/D=1 case is believed to be small. Figure 17 shows the noise around the observer grid for the RMAC and CFD cases with dashed lines again corresponding to the same key high and low points. The RMAC case shows the same directivity pattern observed for H/D = 1, with 6 high noise regions and 6 low noise regions, with a max difference of 15.5 dB that is comparable to the 13.5 dB max difference found for H/D = 1. When aerodynamic interactions are introduced through the CFD loads, the results change considerably. While the directivity pattern remains, with 6 regions of high noise and 6 of low noise, the difference between these peaks and troughs are much lower on average due to the increased interaction with the ground that interferes with the amplification/cancellation patterns observed with the RMAC loads. Looking at the minimum difference between peaks and troughs gives 11 dB for RMAC loads, but this drops to 3.5 dB for CFD loading. There is also a very pronounced difference between the left and right side of the observer grid, with point E being 5.5 dB higher than its mirrored location on the right side, and point C being 4.5 dB higher than its mirrored location. This is due to the increased asymmetry in rotor loading that is caused by the interactional effects. Unlike the case of H/D = 1, where weaker interactions did little to effect the OASPL in dB over the observer grid, the stronger interactions cause more significant differences.

Figure 18 gives the pressure time history at point A for the two different cases (RMAC and CFD) over a single rotor revolution. The pressure time history for the RMAC loads looks very similar for H/D = 0.5 and H/D = 1, with a 6/rev signal. When looking at the CFD loads, the pressure signal looks very different. The pressure exhibits a 3/rev dominant signal, with many other frequencies observable. The loading noise is also the overwhelmingly dominant noise source, with peaks and troughs that are up to 4 times greater than the thickness noise. Thus there is an increase of 7.3 dB at point A when aerodynamic interactions are considered for H/D = 0.5.

Next, ground reflections are introduced into the noise signal. For H/D = 0.5 the rotors that supply the reflection noise are closer to the observers due to the source rotors being closer to the ground. Figure 19 gives the noise around the observer grid for the RMAC and the CFD cases with ground reflections. The OASPL without reflections is also included for comparison. The RMAC case shows similar results to the H/D = 1 case, with a general increase in the noise across the observer grid. A maximum increase of 1.5 dB is observed at point E and its mirrored point. For the CFD case, the results with reflections show a much larger increase in the noise across the observer grid. The directivity is still present when compared to the results using RMAC loads, but the deep lows shown for RMAC loads are no longer present with CFD loads. In fact, the low observed at point G is almost entirely erased, increasing by 8 dB when reflections are added. Again, it appears that the increased aerodynamic interactions interfere with the amplification/cancellation patterns observed with RMAC loads.

To better understand how the reflection noise impacts the H/D = 0.5 cases, we can look at the pressure time history over a rotor revolution as shown in Figure 20. The RMAC results remain similar to previous cases, but the effects of increased interactions are apparent for the CFD results. The loading noise is substantially more dominant than what was observed

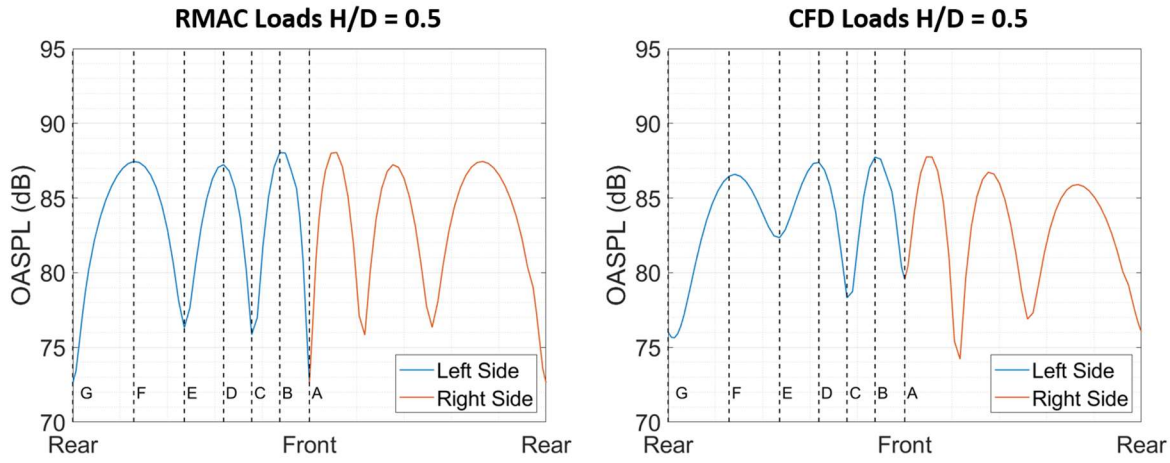

Figure 17: OASPL dB noise at observer grid for H/D = 0.5, no ground reflections

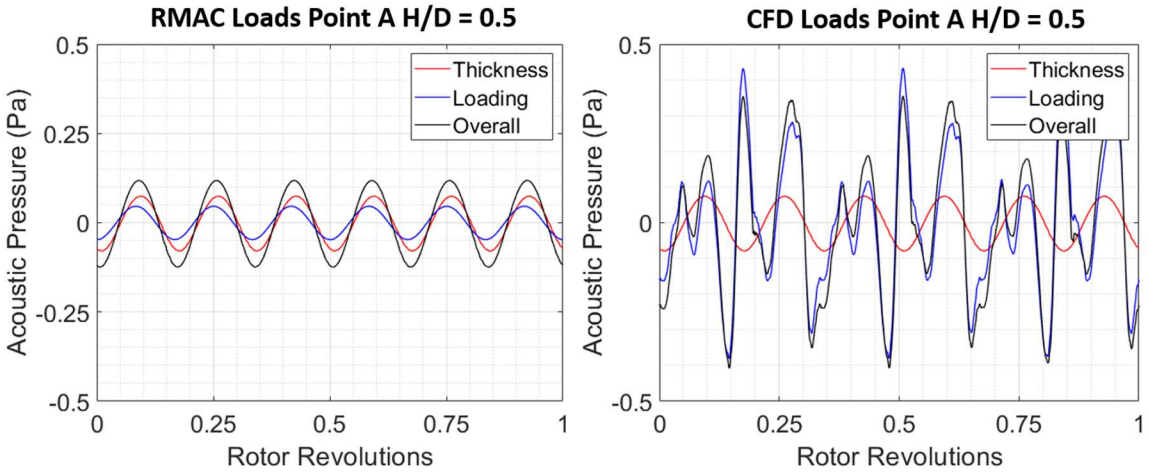

Figure 18: Acoustic pressure time history for H/D = 0.5 at point A (left) RMAC loads (right) CFD loads, no ground reflections

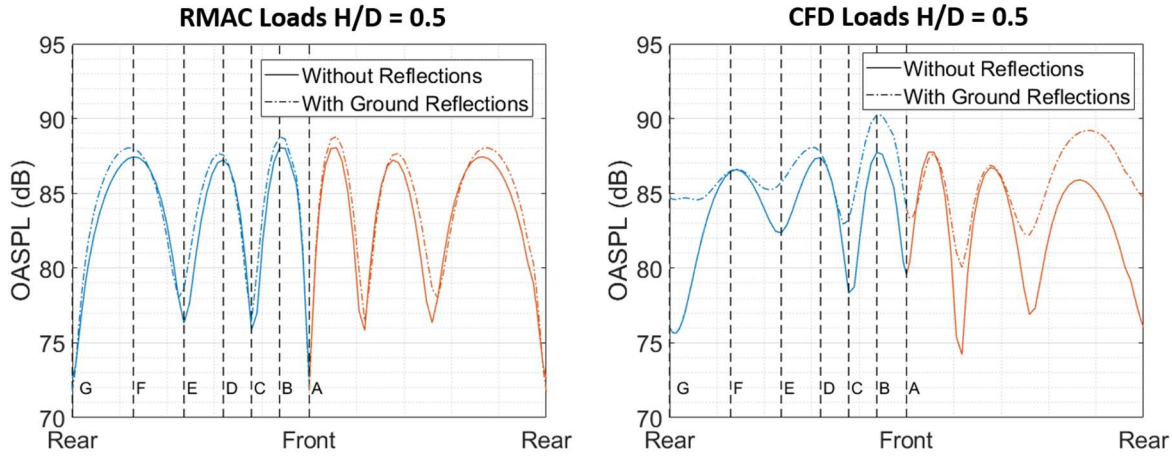

Figure 19: OASPL dB noise at observer grid for H/D = 0.5, including ground reflections

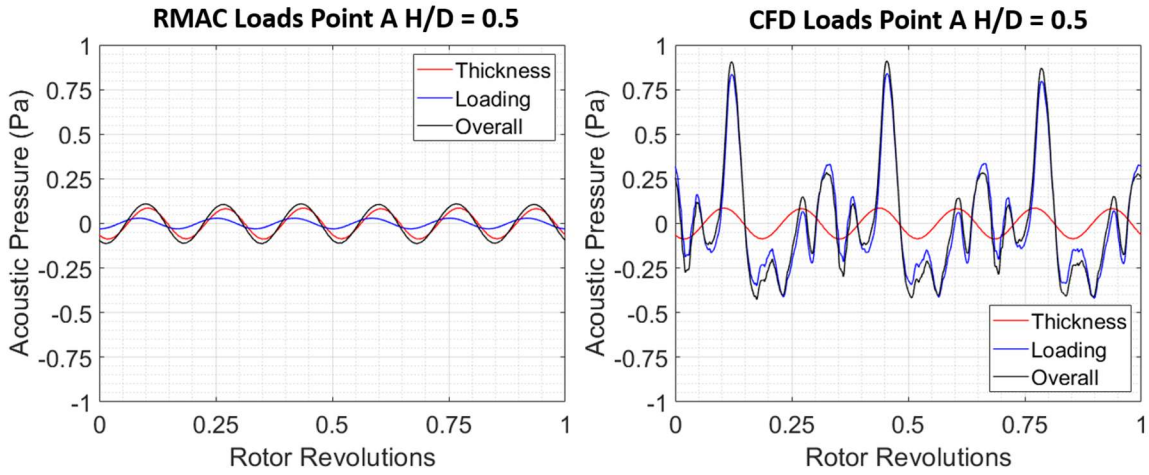

Figure 20: Acoustic pressure time history for H/D = 0.5 at point A (left) RMAC loads (right) CFD loads, including ground reflections

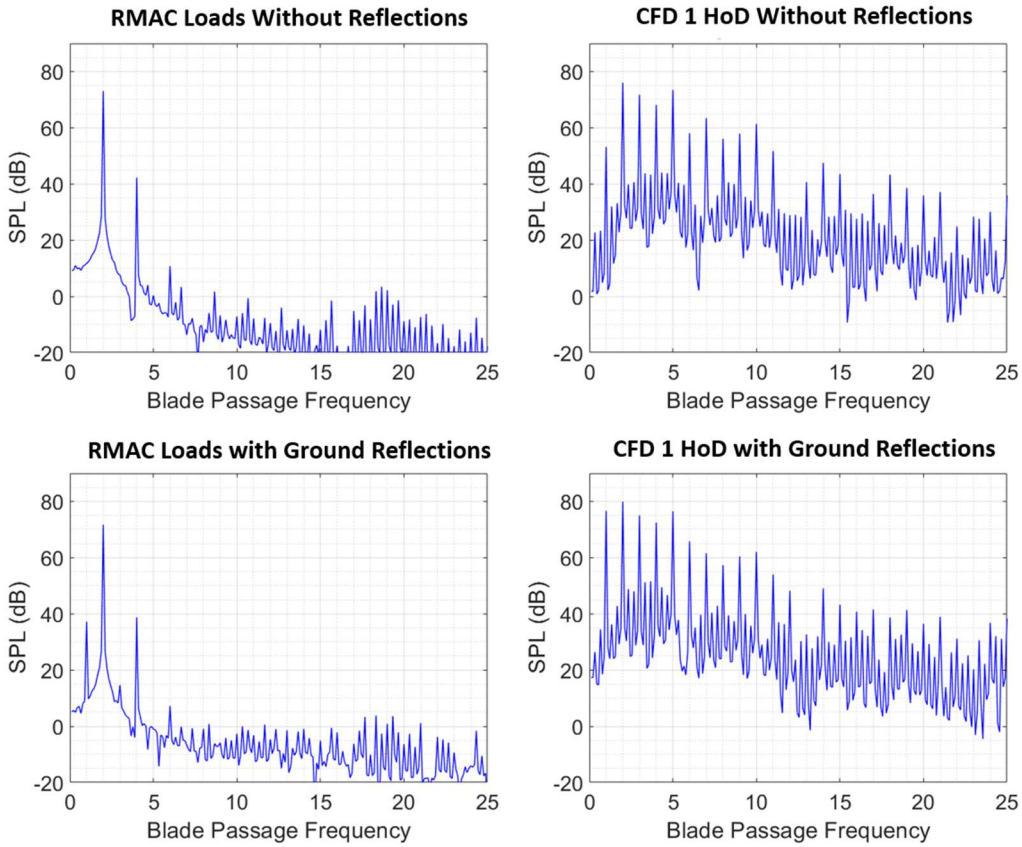

Figure 21: SPL frequency breakdown for Point A H/D = 0.5 (top left) RMAC loads no reflections (top right) CFD loads no reflections (bottom left) RMAC loads with ground reflections (bottom right) CFD loads with ground reflections

without ground reflections in Figure 19. Peaks of 10 times the magnitude of the thickness noise are observed.

The signal is 3/rev dominant, with large variations that are significant contributors of high frequency noise which will show up in the SPL frequency analysis. Therefore, the increased aerodynamic interactions along with ground reflections create a significant increase in the loading noise.

The SPL frequency breakdown is shown in Figure 21 for point A, for both the RMAC and CFD cases with and without ground reflections. The high frequency content observed in the pressure signals is apparent in these figures. As also shown for H/D = 1, the RMAC cases show the peak noise signal at the 2nd BPF. The CFD case without ground reflections for H/D = 0.5 is not strictly 2nd BPF peak dominant, with peaks along the 3rd, and 5th BPF being within 5 dB. This is different when compared to H/D = 1, where 2nd BPF peak was over 10 dB greater than other peaks. For H/D = 0.5 large noise peaks are observed through the 25th BPF due to the aerodynamic interactions. The CFD case with ground reflection shows a similar result, along with another peak close to the dominant peak at the 1st BPF. Again, these peaks are much closer to the dominant peak than was seen in H/D = 1.

Table 3: dB, dBA, and 6th to 25th BPF Noise for Points A and B, H/D = 0.5

RMAC Loads no Reflections

Point	dB	dBA	6th to 25th BPF
A	72.5	59.4	13.8
B	86.9	64.7	24.3

CFD Loads no Reflections

Point	dB	dBA	6th to 25th BPF
A	79.8	61.1	56.5
B	86.5	72.8	69.7

RMAC Loads with Ground Reflections

Point	dB	dBA	6th to 25th BPF
A	71.8	58.5	15.8
B	88.7	65.2	25.3

CFD Loads with Ground Reflections

Point	dB	dBA	6th to 25th BPF
A	88.9	75.3	67.3
B	90.2	74.5	69.3

Values for OASPL dB, dBA, and 6th to 25th BPF content are shown in Table 3. Beginning with the comparison of RMAC and CFD loads without ground reflections, the noise is comparable at point B, but point A is 7.3 dB greater for the CFD case. When A-weighting is applied, the noise at point A is 1.6 dBA higher and at point B is 8.l dBA higher, which is very different when compared to H/D = 1 where the difference was within 1 dBA. This difference between the RMAC and the CFD loads without reflections is greater when comparing noise between the 6th and 25th BPF, where the difference is 42.7 dB for point A and 45.4 dB for point B in H/D = 0.5. This is much greater than what was shown for H/D = 1, where the difference was 20.7 dB for point A and 27 dB for point B. The much greater interactions that are present for H/D = 0.5 cause larger noise peaks at higher frequencies and justify these value differences (in the 6th to 25th BPF dB). When ground reflections are added, the difference is increased at point A to 51.5 dB and slightly decreases at point B to 43.1 dB. Again, ground reflections have an impact on the higher frequency noise, but the dominating source of this high frequency noise is the aerodynamic interactions, and as shown in the H/D = 0.5 case, when the strength of these interactions increases, the high frequency noise increases. The increased aerodynamic interactions in the H/D case create a bigger wake breakdown and a higher high frequency content.

4. CONCLUSION

This study examines the acoustic behavior of hovering two-rotor system in close operation to the ground. The rotors are examined for two heights, H/D = 1 and H/D = 0.5. Loads that include aerodynamic interactions between rotors and between the rotors and ground plane were generated using the CFD solver AcuSolve. Loads with no aerodynamic interaction were also generated using the Rensselaer Multicopter Analysis Code (RMAC) to be used as a point of comparison. Both these loads are provided as inputs to the acoustic propagation code PSU-WOPWOP to evaluate the acoustic pressure time history at select observer locations. The pressure history is then used to calculate the overall sound pressure level (OASPL) at an observer grid located at "ear height" 5 feet above the ground. Rotors are then added below the ground, simulating perfect acoustic reflections off the ground plane. From these simulations the following conclusions can be drawn:

1. The noise signal from the two rotors has a distinct directivity pattern due to the phasing of the arrival times of the signals from the two rotors.
2. The introduction of aerodynamic interactions causes a large increase in high frequency noise. Interaction effects are not readily visible for H/D = 1 when observing OASPL in dB, but when looking at the 6th to 25th BPF range the noise increase is 27 dB at point A and 20.7 dB at point B when compared to loads without aerodynamic interactions. The stronger the interactions, the greater this high frequency noise increase, with the H/D = 0.5 case showing an even greater jump of 42.7 dB and 45.4 dB. Strong wake interactions increase unsteadiness and thus have a substantial effect on the loading noise, increasing it significantly, as well as causing the above-mentioned increase of the noise signal high frequency content.
3. The introduction of ground reflections increased noise across the observer grid and enhanced the high frequency content found in the noise generated by the aerodynamic interactions. Specifically, at high frequency noise at point A the increased 8.7 dB for H/D = 1 and 14.8 dB for H/D = 0.5 when ground reflections were introduced. This effect is meaningful but still not nearly as large as the

increase in high frequency noise that is due to the presence of the aerodynamic interactions. This enhancement in the high frequency content is coupled with additional increases in the loading noise.

ACKNOWLEDGEMENTS

This work was funded in part under the Army/Navy/NASA Vertical Lift Research Center of Excellence (VLRCOE) Program, grant number W911W61120012, with Dr. Mahendra Bhagwat as Technical Monitor.

REFERENCES

1. Holden, J., and Goel, N., "Fast-Forwarding to a Future of On-Demand Urban Air Transportation." UBER Elevate Whitepaper, October 2016, available at: https://www.uber.com/elevate.pdf [Accessed 10 Oct. 2019].
2. Swartz, K., "NASA Embraces Urban Air Mobility," Vertiflite Magazine, Jan-Feb 2019. Pages?
3. Schmitz, F., "The Challenges and Possibilities of a Truly Quiet Helicopter: 29th Alexander A. Nikolsky Honorary Lecture," *Journal of American Helicopter Society*, Vol. 61, No.4, 2016, pp. 1-33.
4. Zawodny, N. and Boyd, D. D., "Investigation of Rotor-Airframe Interaction Noise Associated with Small-Scale Rotary-Wing Unmanned Aircraft Systems," 73rd Annual Forum of the American Helicopter Society, Fort Worth, TX, 2017.
5. Pettingill, N. and Zawodny, N., "Identification and Prediction of Broadband Noise for a Small Quadcopter," 75th Annual Forum of the Vertical Flight Society, Philadelphia, PA, 2019.
6. Schiller, N., Pascioni, K., and Zawodny, N., "Tonal Noise Control Using Rotor Phase Synchronization," 75th Annual Forum of the Vertical Flight Society, Philadelphia, PA, 2019.
7. Thurman, S. C., Zawodny, S. N., Baeder, D. J., "Computational Prediction of Broadband Noise from a Representative Small Unmanned Aerial System Rotor," 76th Annual Forum of the Vertical Flight Society, Virtual, 2020.
8. Pascioni, K. A., Rizzi, S. A., and Schiller, N.H., "Noise reduction potential of phase control for distributed propulsion vehicles," Paper AIAA 2019-1069, AIAA SciTech Forum and Exposition Proceedings, San Diego, CA, January 2019.
9. Tinney, C. and Sirohi, J., "Multirotor Drone Noise at Static Thrust," *AIAA Journal*, Vol. 56, No. 7, pp. 2816-2826, July 2018.
10. Tinney, C. and Valdez, J., "Acoustic Scaling for Small Rotors in Hover," 75th Annual Forum of the Vertical Flight Society, Philadelphia, PA, 2019.
11. Intaratep, N., Alexander, W., and Devenport, W., "Experimental Study of Quadcopter Acoustics and Performance at Static Thrust Conditions," *22nd AIAA/CEAS Aeroacoustics Conference*, Lyon, France, May 2016.
12. Passe, B. and Baeder, J., "Computational Aeroacoustics of Different Propeller Configurations for eVTOL Applications," *Vertical Flight Society's Autonomous VTOL Technical Meeting and Electric VTOL Symposium,* Mesa, Arizona, Jan. 2019.
13. Quackenbush, T., Wachspress, D., Moretti, L., Barwey, D., Lewis, R., and Brentner, K., "Aeroacoustic Modeling of an eVTOL Slowed Rotor Winged Compound Aircraft," *75th Annual Forum of the Vertical Flight Society,* Philadelphia, PA, May 2019.
14. Jia, Z., and Lee, S., "Acoustic Analysis of Urban Air Mobility Quadrotor Aircraft," *Vertical Flight Society's Transformative Vertical Flight Forum*, San Jose, CA, Jan 21-23, 2020
15. Wachspress, D., Yu, M., and Brentner, K., "Rotor/Airframe Aeroacoustic Prediction for eVTOL UAM Aircraft," *75th Annual Forum of the Vertical Flight Society,* Philadelphia, PA, May 2019
16. Li, S., and Lee, S., "UCD-QuietFly: A New Program to Predict Multi-Rotor eVTOL Broadband Noise" *Vertical Flight Society's Transformative Vertical Flight Forum*, San Jose, CA, Jan 21-23, 2020.
17. Mankbadi, R. R., Afari, S. O., and Golubev, V. V., "Simulations of Broadband Noise of a Small UAV Propeller," AIAA paper 2020-1493, AIAA SciTech Forum, Orlando, FL, January 2020.
18. Zawodny, N., Boyd, D. D., and Burley, C., "Acoustic Characterization and Prediction of Representative, Small-Scale Rotary-Wing Unmanned Aircraft System Components," *72nd Annual Forum of the American Helicopter Society,* West Palm Beach, FL, May 2016.
19. Lee, S., Shlesinger, I., "Coaxial Rotor Broadband Noise Prediction in Hover," 76th VFS Annual Forum, Virginia Beach, VA, 2020
20. Jia, Z., Lee, S., "Aeroacoustic Analysis of a Side-by-Side Hybrid VTOL Aircraft," 76th VFS Annual Forum, Virginia Beach, VA, 2020
21. Alvarez, J. E., Schenk, A., Critchfield, T., Ning, A., "Rotor-on-Rotor Aeroacoustic Interactions of Multirotor in Hover," 76th Annual Forum of the Vertical Flight Society, Virginia Beach, VA, 2020
22. Jacobellis, G., Singh, R., Johnson, C., Sirohi, J., McDonald, R., "Experimental and Computational Investigation of Stacked Rotor Acoustics in Hover," 76th VFS Annual Forum, Virginia Beach, VA, 2020
23. Niemiec, R. and Gandhi, F., "Development and Validation of the Rensselaer Multicopter Analysis Code (RMAC): A Physics-Based Comprehensive Modeling Tool," *75th Annual Forum of the Vertical Flight Society,* Philadelphia, PA, May 2019.

24. M. Misiorowski, F. Gandhi, and A. A. Oberai, "Computational Study on Rotor Interactional Effects for a Quadcopter in Edgewise Flight," *AIAA Journal*, Vol. 57, No. 12, December 2019, pp. 5309-5319; https://doi.org/10.2514/1.J058369.
25. Altair Engineering Inc., Modeling of Turbulence - Near-Wall Modeling. acu-solve/training manual/near wall modeling, 2019.
26. Y. Bazilevs, C. Michler, V. Calo, and T. Hughes, "Weak Dirichlet Boundary Conditions for Wall-Bounded Turbulent Flows," *Computer Methods in Applied Mechanics and Engineering*, vol. 196, no. 49, pp. 4853 – 4862, 2007.
27. R. Healy, M. Misiorowski, and F. Gandhi, "A Systematic CFD-Based Examination of Rotor-Rotor SeparationEffects on Interactional Aerodynamics for Large eVTOLAircraft," Proceedings of the 75th VFS Annual Forum, Philadelphia, PA, May 2019.
28. R. Healy, F. Gandhi, M. Mistry, and M. Duffy, "A Computational Investigation of Multi-rotor Interactional Aerodynamics with Hub Lateral and Longitudinal Canting," Proceedings of the 76th VFS Annual Forum, (Virtual), October 2020.
29. R. Healy, J. McCauley, F. Gandhi, O. Sahni, and M. Mistry, "A Computational Investigation of Side-by-Side Rotors in Ground Effect," Proceedings of the 77th VFS Annual Forum, (Virtual), y, May 2021.
30. Brentner, K., Bres, G. A., and Perez, G., "Maneuvering Rotorcraft Noise Prediction: A New Code for a New Problem," *AHS Aerodynamics, Acoustics, and Test and Evaluation Technical Specialist Meeting,* San Francisco, CA, Jan. 2002.